Characteristics of ore minerals associated with gold at the Prestea mine, Ghana

NAPOLEON Q. HAMMOND

Geological Institute, University of Tokyo, 7-3-1 Hongo, Tokyo 113, Japan

AND

HIROKAZU TABATA

Department of Earth and Planetary Sciences, Tokyo Institute of Technology, Ookayama, Meguro-ku, Tokyo 152, Japan

Abstract

Gold in Early Proterozoic Birimian greenstone at Prestea in Ghana is associated with base metal sulphides and sulphosalts including arsenopyrite, pyrite, sphalerite, chalcopyrite, pyrrhotite, galena, tetrahedrite, bournonite, boulangerite and jamesonite. The occurrence of the gold is intimately associated with arsenopyrite and the sulphosalts, and to a lesser extent with the other sulphides. The tetrahedrites at Prestea constitute the major component of sulphosalts associated with gold and occurring in two distinct types. Type I show ideal stoichiometric composition. Type II tetrahedrites deviated from the ideal stoichiometry and are represented approximately by the average formula $(Cu,Ag)_{9.61}(Fe,Zn)_{2.39}(Sb,As)_4S_{13}$. The tetrahedrites co-precipitated with gold exhibit ideal characteristics indicating an equilibruim state of the mineralizing fluid during precipitation. Three types of pyrites were distinguished by electron-microprobe analyses based on their As, Co and Ni composition. The As content in type I vary from 0.15 to 0.37 wt%, and contain up to 2 wt.% Co.Type II pyrites are As-rich and form the most dominant with As content ranging from 0.2 to 2.69 wt.%. Ni content varies from below-detection to 1000 ppm. Type III pyrites are poor in the trace elements and consistent with the stoichiometric composition. The mineralization occurred in three paragenetic stages from at least a two-phase hydrothermal fluid, with stage II forming a prolonged and main stage of the ore and gold mineralization. Redox changes in ore fluid which were triggered by episodic pressure releases during fissuring and fracturing caused fluctuation of the activity of the As/Ni ratio and subsequent oscillatory zoning of Ni in As-rich ores.

KEYWORDS: ore minerals, gold, greenstone, Prestea, Ghana.

Introduction

IN Ghana, gold mining forms a major economic venture and has contributed significantly to the economic development of the country. The gold occurs in Early Proterozoic Birimian greenstones which bear much similarity with most Archaean greenstone deposits, particularly in terms of its high gold potential. The gold mineralization is most prominent along the western margin of the Ashanti belt (Fig. 1). Despite its widespread occurrence and large mining activities, documentation on gold in the Birimian is limited. Nearly two decades ago, the genesis of gold in the Birimian was not well understood. In recent years, several workers including Ntiamoah-Agyakwa (1979), Bowell (1992), Eisenlohr (1992), Mumin *et al.* (1994), Obethur *et al.* (1994), Mucke and Dzigbodi-Adjimah (1994), Hammond and Shimazaki (1994) have carried out investigations on these deposits involving textural and paragenetic studies, fluid inclusion, stable isotope and other advanced analytical techniques to identify the fluid source, source of gold and other species in the ore fluid, transport and deposition of gold, among others. These studies have contributed significantly to the understanding of gold genesis in the Birimian. In this paper, we present another contribution based on the mineralogical and

Mineralogical Magazine, December 1997, Vol. 61, pp. 879–894

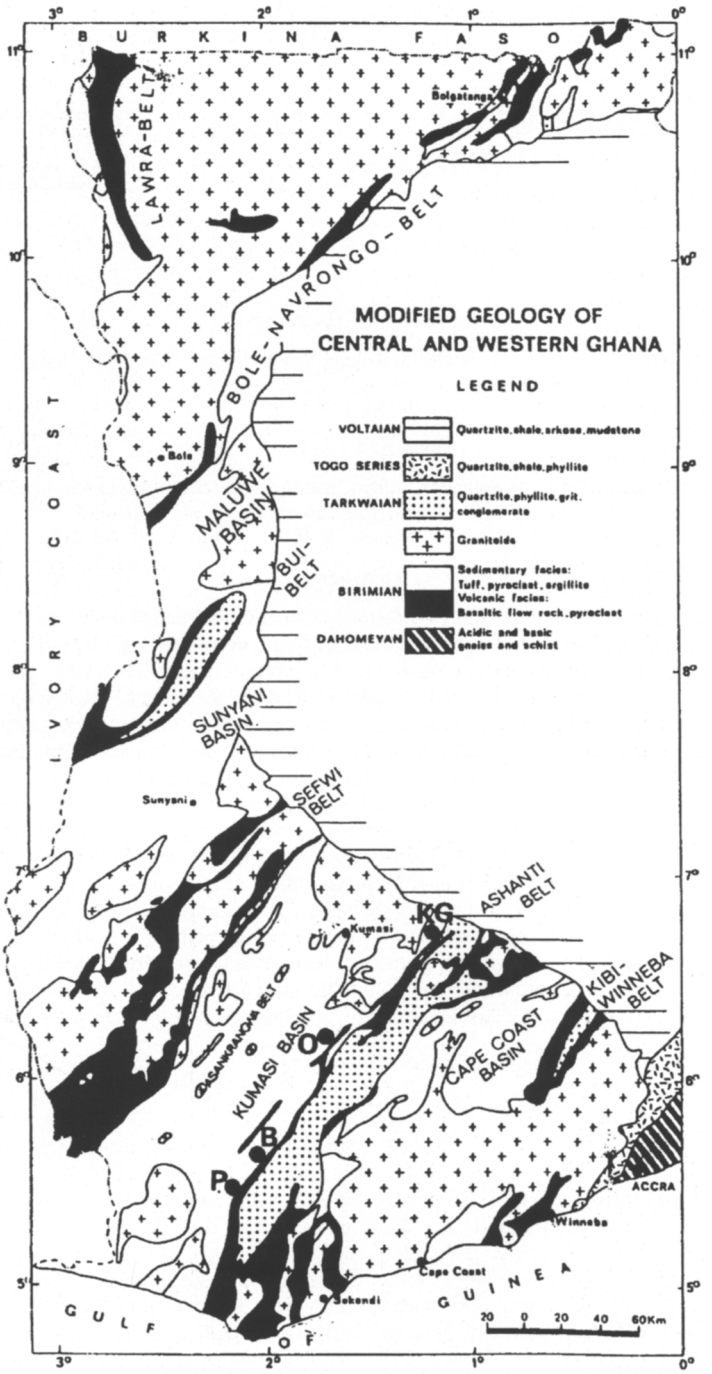

FIG. 1. Geological map of southwestern Ghana showing the position of the Prestes (P), Bogosu (B), Obuasi (O) and the Konongo (KG) gold deposits along the northwestern margin of the Ashanti volcanic belt (Modified after Leube *et al.*, 1990).

geochemical composition of the ore minerals associated with gold at Prestea and a probable paragenetic sequence of mineralization.

Geological setting and mineralization

Early Proterozoic Birimian greenstone assemblages (2100 Ma) constitute the major geologic units in Ghana. They occupy about twenty percent of the total area of Ghana, and form part of the West African craton that outcrops extensively in other parts of the subcontinent, including Cote d'Ivoire, Burkina Faso and Mali. The greenstone units in Ghana are characterized by five evenly spaced volcanic belts trending NE–SW interspersed with sedimentary basins, (Fig. 1). The volcanic rocks range from tholeiitic to acid volcanics, and commonly interbedded with graywackes and carbonaceous phyllites. The sedimentary units consist of shales, silts, greywackes, tuffs and chemical sediments. These rocks have experienced greenschist to amphibolite grade metamorphic facies (Kesse, 1985).

Locally, the Birimian is subdivided into a lower unit of metamorphosed sedimentary rocks and the upper unit composed of volcanic rocks. Tarkwaian clastic sediments (dated 1900 Ma) overlie the Birimian unconformably. Both formations were subjected to the Eburnean thermo-tectonic orogeny resulting in the folding, metamorphism and the introduction of granitoids of diverse chemical composition (Black, 1980). Kesse (1985) and Eisenlohr and Hirdes (1992) have described in detail the characteristics of these granitoid suites, namely Cape Coast, Dixcove, Winneba and Bongo granites. Geochronological dating of these granitoids range between 2.18 and 2.17 Ga (Hirdes *et al.*, 1992). The Birimian volcanics have been dated at 2166 ± 66 Ma by Taylor *et al.* (1992). Davis *et al.* (1994) also dated Birimian metasediments between 2184 and 2135 Ma.

The Prestea gold mine is located in the southwestern section of the Ashanti gold belt of the Birimian which trends in an NE–SW direction (Fig. 2). The belt represents an important carbonaceous shear zone hosting major mining companies, and accounts for over 60% of total gold production in Ghana. Two types of gold mineralization are identified in the Birimian: a quartz-vein type with gold occurring as native gold, and as disseminated gold in sulphide ore, where the gold occurs as submicroscopic grains in the sulphide ores. Gold production at Prestea is limited to the quartz lodes. A main reef and two subsidiary reefs hosted in carbonaceous metasediments constitute the quartz lodes at Prestea. Based on their textures, four types of quartz veins have been identified; smoky quartz characterized by fragments of host rock and

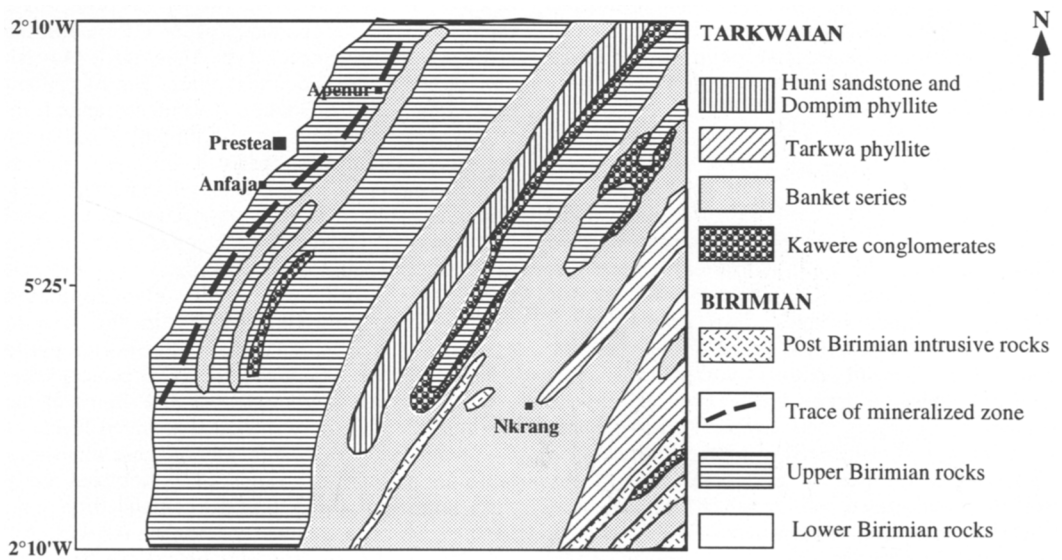

FIG. 2. Geology and location map of Prestea mine area (modified after a Prestea mine drawing).

laminations of cabonaceous materials, massive quartz with disseminated sulphides, grey to white laminated quartz and glassy massive white quartz. This study focuses on the smoky quartz which carries the bulk of gold mined at Prestea. Deep mining has been developed to depths of about 1.6 km along the main fissure.

Analytical methods

Auriferous quartz samples from various mining levels of the Prestea deposit were examined by reflected light in polished sections, and the paragenesis of the ore minerals was determined based on their textures and assemblage. The compositions of the minerals in selected samples were analysed by electron microprobe at the Tokyo Institute of Technology and the University of Tokyo. Operating conditions were 25 kV at 30 nA, 100 s counting time for Ni and Co, and 20 s for all other elements. Backscattered imaging was applied to investigate any heterogeneity in ore minerals. Systematic map analyses across grains were also conducted at 25 kV and 60 nA, to verify the spatial distribution of specific elements in zoned samples.

Ore mineralogy and mineral chemistry

The ore minerals associated with gold consist of base metal sulphides and Sb-bearing suphosalts. Arsenopyrite, pyrite, chalcopyrite, sphalerite, pyrrhotite and galena are the principal sulphide minerals present. The sulphosalts include tetrahedrite, boulangerite, bournonite and jamesonite. In addition, ullmanite and gersdoffite were observed in trace amounts.

Sulphides

Arsenopyrite forms the most dominant sulphide phase occurring with gold at Prestea. It occurs as euhedral to subhedral crystals with characteristic rhombic to angular shapes. Two generations of arsenopyrite were identified based on their textural relationships. The early phase is readily identified by the coarse and large grains greater than 100 μm and common fracturing in most samples (Fig. 4A). This fracturing may be attributed to a later deformational event. Arsenopyrites is also characterized by oscillatory and growth zoning which in most cases, reflects the variation in As content. The As content generally increases from core to rim in zoned samples. Systematic map analyses across some grains revealed variable Ni contents alternating from core to rim (Fig. 5A). High levels of Co up to 3 wt.% were observed in growth zones along the margins of some arsenopyrites. But total Ni and Co in analysed grains were less than 0.2 wt.%. Inclusions of rutile or ilmenite are common in some crystals. Later formed arsenopyrite is characterized by fine and smaller grains less than 300 μm and free of inclusions. They occur as isolated grains or coexist with other sulphides and sulphosalts. In places, they occur as aggregates in a continuous array, probably indicating the direction of shear during recrystallization. Zoning is present in some crystals on a small scale mainly due to variation in As irregularly across the grains. Gold is intimately associated with these arsenopyrite along grain boundaries and in cracks in the arsenopyrite (Fig. 4B).

Pyrite is the second most abundant ore mineral after arsenopyrite. It generally occurs as euhedral coarse to fine grains and ranging in size from 50 μm to 3 mm. Alteration of pyrite to marcasite is commonly observed. On the basis of their trace element composition As, Co and Ni, three types I, II and III were distinguished by microprobe analyses. Representative data are presented in Table 1 and illustrated in Fig. 6.

Type I pyrite is Co-rich and homogeneous. It contains up to 2 wt.% Co with average value of 1.8 wt.%, and As composition averaging 0.2 wt.%. The type I pyrite is rare and may be attributed to a local occurrence; however its occurrence provides useful information on the paragenesis of the ore mineral assemblage. Identified type I pyrite form the core of type II pyrite (Fig. 3C). A sharp compositional boundary exists between the two pyrites reflecting a rapid change in the chemistry of the ore fluid in the crystallization sequence. Type II pyrite is As-rich and forms the most dominant phase. The As content range from 0.2 to 2.69 wt.%. Ni contents range from below detection-limit to 1000 ppm. Oscillatory zoning is commonly observed in these As-rich pyrites. Microprobe point analyses indicated variation of As content in each zone. There is a general decrease in As content from the core to rim in most of these pyrite grains. A systematic map analyses across some of these grains also indicated oscillating concentrations of Ni in the As-rich pyrites (Fig 5B). In some cases, the As-rich pyrite contains several inclusions, mostly of chalcopyrite, arsenopyrite and pyrrhotite (Fig. 3A). Some of the arsenopyrite inclusions indicated elevated levels of Co up to 2 wt.% in growth zones. These inclusions presumably represent relics of remobilzed early formed minerals. Type III pyrite contains little or no trace element content and has less than 0.2 wt.% As. The Ni and Co contents are below the detection limit of microprobe analyses. The pyrite occurs as discrete grains or as overgrowths on the As-rich type II pyrite (Fig. 3A and B). They exhibit various shapes and sizes and have a uniform composition.

TABLE 1. Representative microprobe analyses of pyrites (wt.%)

Type I (Co-rich) Sample point	Fe	Co	As	S	Total
SQ2.91	44.52	1.85	0.21	53.55	100.13
SQ2.92	44.55	1.8	0.15	53.44	99.94
SQ2.93	44.43	1.9	0.19	53.7	100.22
SQ2.9	44.37	1.91	0.28	53.63	100.19
SQ2.10	44.69	1.77	0.23	53.56	100.25
SQ2.11	44.84	1.48	0.15	53.49	99.96
SQ3.3	44.27	2	0.37	53.05	99.69
Type II (As-rich)					
Sample point	Fe	Ni	As	S	Total
3SQ2.100	46.91	0.09	0.44	53.25	100.69
4SQ2.108	46.79	0.04	0.35	54.19	101.37
4SQ2.1	46.64	0.08	0.49	53.65	100.86
4SQ2.2	46.53	0.05	0.44	53.5	100.52
5SQ2.7	46.38	0.04	0.31	53.23	99.96
5SQ2.8	46.77	0.04	0.22	53.78	100.81
SQ3.1	46.11	–	0.51	52.99	99.61
SQ3.2	46.02	–	1.03	52.41	99.46
SQ4B10	46.04	0.08	0.59	53.2	99.91
2SQ2.13	45.84	–	0.53	53.51	99.88
SQ4.1	45.72	0.1	0.66	52.26	98.74
SQ4.12	46.72	–	0.33	53.06	100.11
SQ4.13	46.51	–	0.41	53.14	100.06
SQ5.1	46.09	0.06	0.36	52.65	99.16
2SQ5.8	45.81	0.02	0.29	52.87	98.99
2SQ2	45.67	0.06	2.69	51.38	99.8
2SQ2.11	46.32	0.04	0.82	53.37	100.55
3SQ3.16	46.46	0.1	0.63	52.47	99.66
4SQ2.2	46.64	0.03	0.18	54.35	101.2
Type III (Normal pyrite)					
Sample point	Fe	Ni	As	S	Total
3SQ2.101	46.98	–	0.06	53.86	100.9
3SQ2.102	46.87	–	0.12	53.4	100.39
4SQ2.106	46.73	–	0.23	53.38	100.34
4SQ2.107	46.77	–	0.08	53.99	100.84
4SQ2.4	46.96	–	0.11	54.04	101.11
4SQ2.4	46.96	–	0.11	54.04	101.11
5SQ2.5	46.82	–	0.13	53.24	100.19
5SQ2.6	46.55	–	0.12	53.32	99.99
SQ3.5	46.45	–	0.16	53.22	99.83
1SQ3.6	46.48	–	0.08	53.43	99.99
SQ3.12	46.04	0.03	0.08	53.1	99.25
SQ4B6.45	45.85	0.1	–	53.5	99.45
2SQ5.12	46.87	–	–	53.34	100.21
2SQ5.10	46.07	–	–	53.88	99.95

Some type III pyrites have been subjected to fracturing. In a previous study, Mumin *et al.* (1994) reported overgrowth of As-rich pyrite on As-poor pyrite. This observations we interpret to mean the As-poor pyrite crystallization occurred in two stages at Prestea.

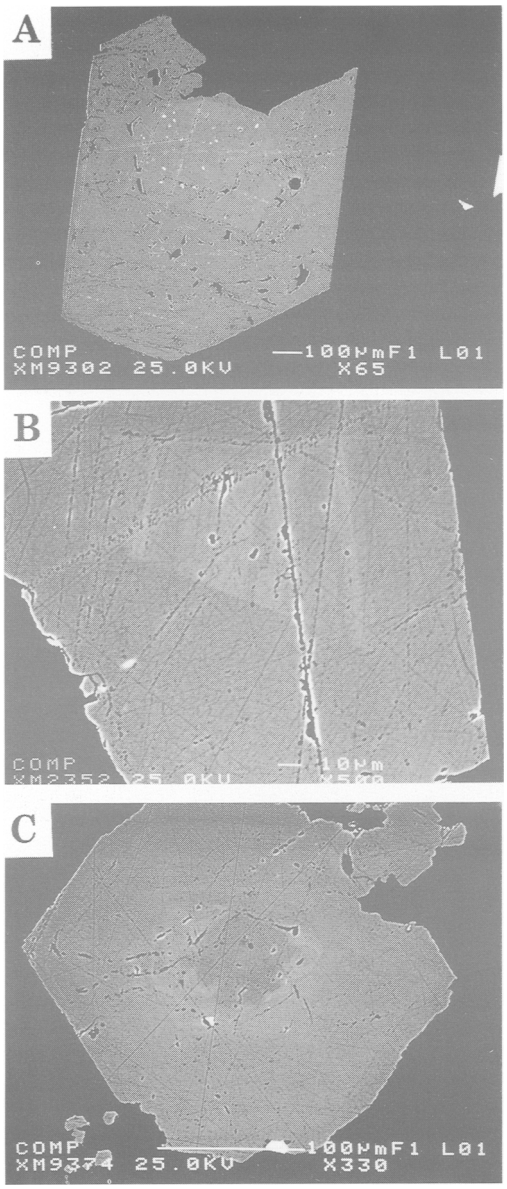

FIG. 3. Back scattered electron images of the three forms of pyrite at the Prestea gold deposit. (A) Inclusion-filled type II pyrite overgrown by type III pyrite. (B) - Oscillatory zoned type II pyrite overgrown by type III pyrite (oscillatory zoning is due to variation in As content). (C) Overgrowth of type II pyrite on type I pyrite (core).

Sphalerite occurs as fine euhedral isolated grains or closely associated with gold, sulphides and sulphosalts. Grain size ranges from less than 50 to about 500 μm. It shows a quite homogeneous composition in each grain but variable from grain to grain in polished section. The Fe content in sphalerite has no detectable variation with the sulphide or sulphosalt association. A range from 0.5 to 4 wt.% Fe was obtained for all analysed grains. A sphalerite inclusion in pyrite attained the highest content Fe of 4.5 wt.%. Cd composition is generally less than 1 wt.%. This variation of Fe in sphalerite is attributed to lack of buffering mineral assemblage and inhibits its use as a geobarometer (Hutchison and Scott, 1981).

Chalcopyrite is common as inclusions in coarse-grained pyrite or intergrown with other sulphide minerals. A few isolated grains were also observed. Generally it has a composition consistent with stoichiometry.

Galena is a minor constituent of the ore assemblage and mostly coexists with the Pb-Sb sulphosalts. It occurs as rounded or lens-shaped inclusions in bournonite or intergrown with boulangerite. Bi and Se were detected in all analysed samples and show a uniform composition with average values of 0.22 and 0.61 wt.% respectively. Sb occurs in all analysed samples with variable compositions up to 0.91 wt%.

Pyrrhotite is a minor component of the ore assemblage occurring as vug fillings or inclusions in pyrite or arsenopyrite. Fe composition varies from 45.0 to 46.7 at.%. Pyrrhotite inclusions in pyrite are relatively enriched in Ni averaging 0.4 wt.% consistent with Ni preferential partitioning in pyrrhotite (Hawley and Nicols, 1961).

Ullmanite, gersdoffite. These Ni-Co-Sb-As-bearing minerals occur in trace amounts in trapped carbonaceous materials in the quartz vein and are mostly associated with pyrite. They are very heterogeneous and largely non-stoichiometric. Ni exhibites a wide compositional range in gersdoffite from 14.85 to 33.24 wt.% and As varies from 32.22 to 44.61 wt.%. Co is also variable from 0 to 7.32 wt.%. The Ni content in ullmanite shows a limited range from 24.26 to 26.19 wt.% and Sb varies from 48.59 to 53.05 wt.%. As in ullmanite ranges from 5.01 to 9.38 wt.%.

Gold commonly occurs as native Au intimately associated with arsenopyrite, the sulphosalts or as isolated grains, and ranges in size up to 200 μm. Some rather rara microscopic gold grains occur associated with other sulphides, particularly sphalerite, pyrite and galena. Gold association with arsenopyrite mainly occurred with the later mineralization phase, filling fractures or developing along the boundary of the grains. No visible gold or microprobe analyses found any evidence of gold

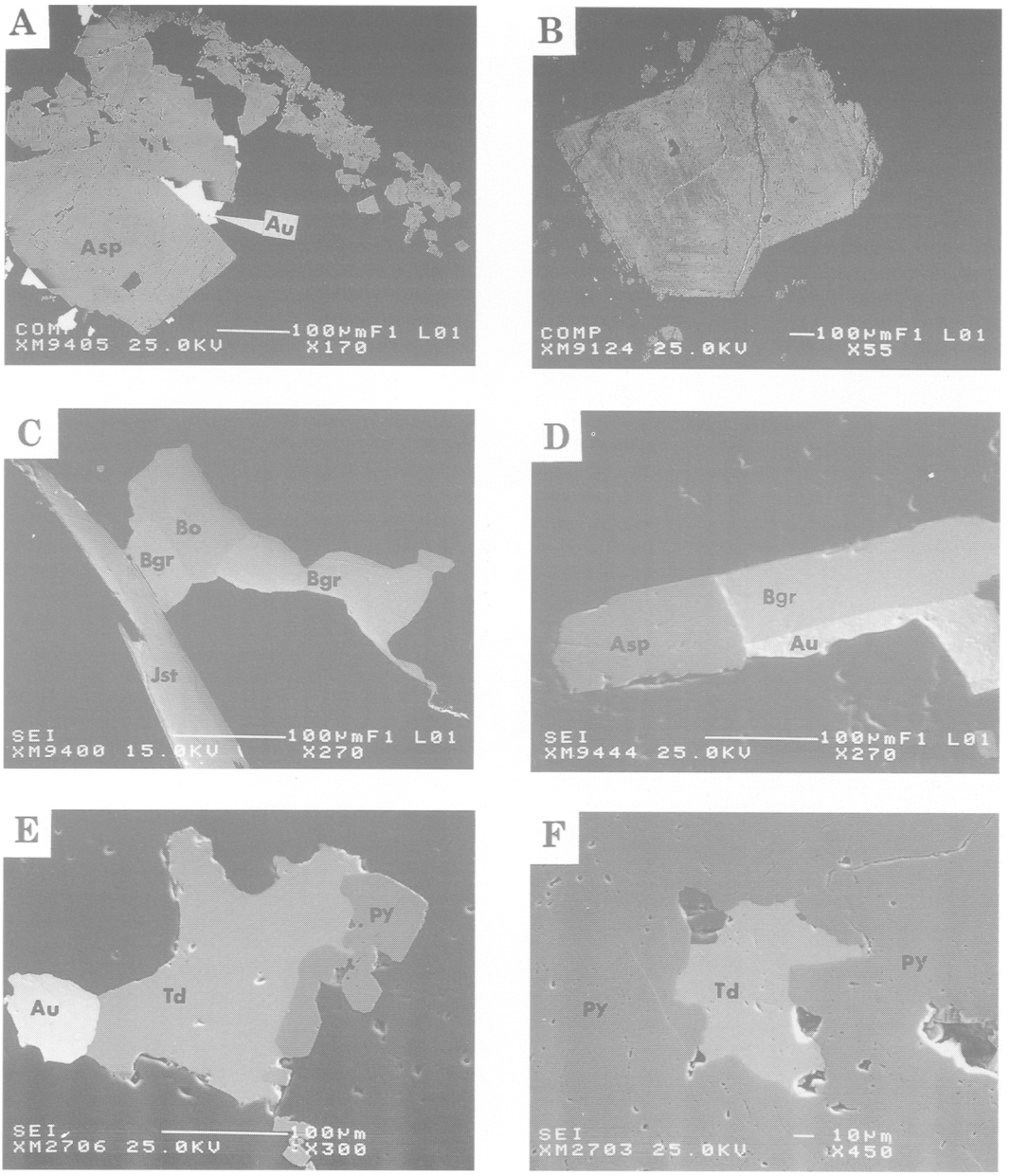

FIG. 4. (A) Back-scattered images showing intimate association of native gold (Au) with arsenopyrite along grain boundaries. Note the continuous array of recrystallized arsenopyrite. (B) Oscillatory zoning of As in early arsenopyrite. (C) Secondary electron image showing co-existing Pb-Sb sulphosalts boulangerite (Bgr), bournonite (Bo), and jamesonite (Jst). (D) Secondary electron image of gold (Au) intergrown with arsenopyrite (Asp) and boulangerite (Bgr). (E) Secondary electron image showing gold (Au) in association with tetrahedrite (Td) and pyrite (Py). (F) Secondary electron image of tetrahedrite (Td) enclosed in pyrite.

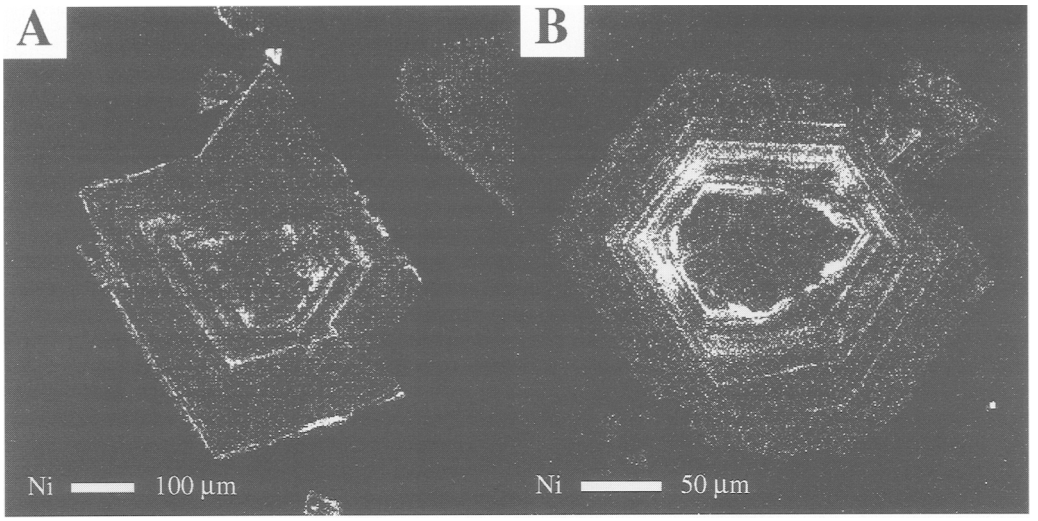

FIG. 5. Electron microprobe traverse across arsenopyrite (A) and As-rich type II pyrite (B) showing similar ascillatory zoning of Ni. (See Fig. 3C for back-scattered image of 'B').

association with the early stage arsenopyrite grains; however the possibility of gold occurring in lattice sites, which cannot be detected by EPMA cannot be ruled out. Gold associated with the sulphosalts also occurs along grain boundaries or precipitated together in quartz fractures. The intimate association of gold with arsenopyrite along the grain boundaries may indicate a coeval precipitation with ore mineralization, or gold released from the crystal lattice of recrystallized arsenopyrite.

Sulphosalts

The sulphosalts include tetrahedrite, boulangerite, jamesonite and bournonite. They are fine grained and

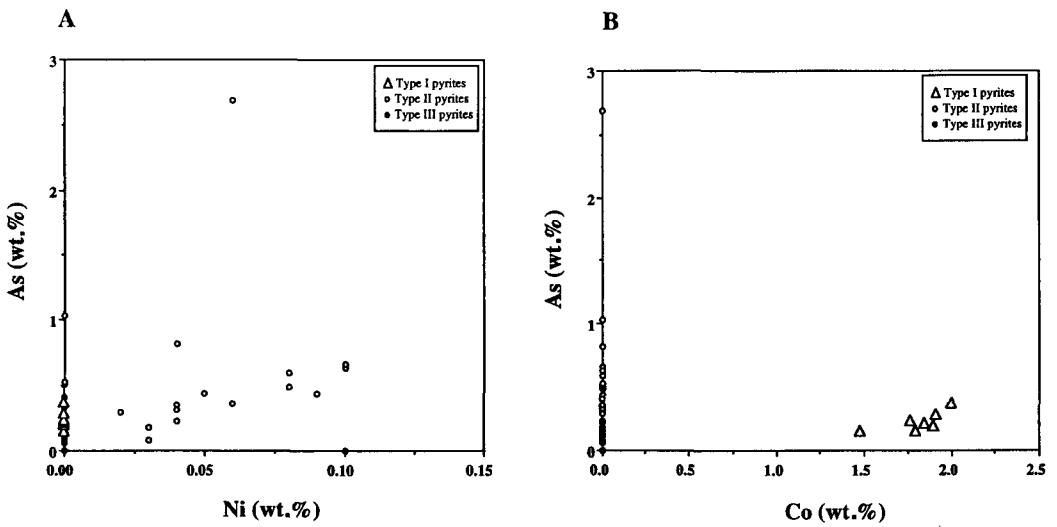

FIG. 6. Plots illustrating the variation of As, Ni and Co in Prestea pyrite. (A) Ni and As and (B) Co and As.

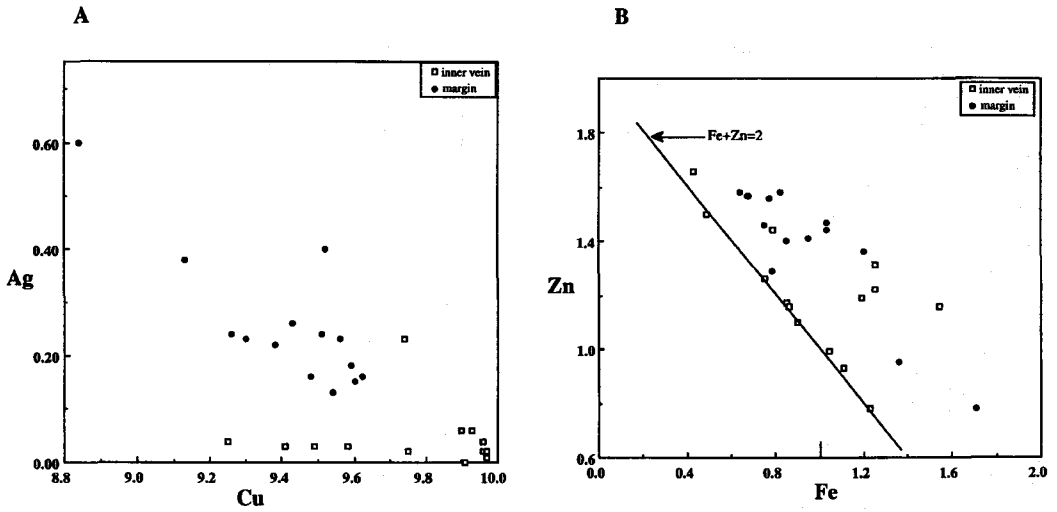

FIG. 7. Compositional variation of (A) Cu and Ag, and (B) Zn and Fe in Prestea tetrahedrites.

occur as isolated grains, coexist or associated with sulphides.

Lead-antimony sulphosalts. Jamesonite, boulangerite and bournonite are the main Pb-Sb sulphosalts (Fig. 4C). They show uniform composition, however variable amounts of Bi occur in these sulphosalts. 0.57 to 1.38 wt.% was detected in jamesonite, 0.47 to 0.73 wt.% in boulangerite and 0.06 to 0.36 wt.% in bournonite. The composition of Se is relatively constant in each sulphosalt with average values of 0.25 wt.% in jamesonite, 0.30 wt.% in boulangerite and 0.35 wt.% in bournonite.Their general formula is represented approximately as $Pb_{4.03}Fe_{0.98}(Sb_{5.84-}Bi_{0.11})_{\Sigma 5.95}(S_{13.93}Se_{0.07})_{\Sigma 14}$ $Pb_{5.01}(Sb_{3.86}Bi_{0.06})_{\Sigma 3.92}(S_{10.93}Se_{0.07})_{\Sigma 11}$ and $Pb_{1.01}Cu_{1.03}Sb_{0.98}(S_{2.98}Se_{0.02})_{\Sigma 3}$ respectively. The occurrence of these Pb-bearing sulphosalts indicates a significant concentration of Pb in the ore fluid.

Tetrahedrite accounts for the greater percentage of the observed sulphosalts at Prestea. It occurs as isolated grains or coexists with the Pb-Sb sulphosalts, sulphides and gold. Pyrite is the most common sulphide mineral intimately associated with tetrahedrite, in close contact or filling interstices in pyrite. Some grains were also observed intergrown with chalcopyrite and sphalerite. The composition of tetrahedrite is quite homogeneous in each grain, but exhibits some variation between each grain in a single polished section. At deeper levels of the mine, tetrahedrite occurs only rarely in the sampled quartz vein, but is relatively common in samples obtained at the 400 and 600 m levels, where it is mostly associated with gold, Pb-Sb sulphosalts and sulphides.

Tetrahedrite chemistry and correlation

Studies on the tetrahedrite–tennantite solid-solution series in ore deposits have provided valuable information on the compositional variation which is attributed to changes in the chemistry of the mineralizing fluid during crystallization, bulk composition of the host rock, co-existing mineral assemblages and variable P–T–f_{O_2} conditions. The spatial variations of the elements in an ore deposit have provided a guide to the compositional changes during crystallization, or the direction of flow of the hydrothermal fluid. These trends have been demonstrated by several authors; Wu and Petersen (1977), Miller and Craig (1983), Hackbarth and Petersen (1984), Lynch (1989). The ideal structural stoichiometry of tetrahedrite-tennanantite is simplified as (O'Leary and Sacks, 1987) $(Cu,Ag)_6^{TRG}$ $[(Cu,Ag)_{2/3}(Fe,Zn)_{1/3}]_6^{TET}(Sb,As)_4^{SM}S_{13}$, where TRG, TET and SM represent trigonal planar, tetragonal and semimetal sites respectively. The chemical formula may be written as $(Cu,Ag)_{10}(Fe,Zn)_2(Sb,As)_4S_{13}$ with possible deviation from the ideal formula due to substitution in metallic sites (Sack and Loucks, 1985; Johnson *et al.*, 1986). Such deviations have been reported in naturally occurring samples by some authors (e.g. Lynch, 1989; Slim-shimi *et al.*, 1996; Miller and Craig, 1983).

In this study, 35 grains of tetrahedrite in auriferous quartz samples from the inner part and margin of the vein with the host rock at the 9 and 12 levels (400 and 600 m respectively below surface) were analysed to assess their compositional variation in the ore

deposit. One tetrahedrite sample SQ28 in the inner vein from the depth of about 1200 m was analysed.

The number of atoms were calculated based on M^{+} + M^{2+} =12 where M^{+} and M^{2+} refer to (Cu+Ag) and (Fe+Zn), respectively, Table 2. The data show low Ag contents up to 3.83 wt.% in all analysed samples. Higher Ag contents (up to 17.4 wt.%) have been identified in samples from deeper sections (1000 m) at the Prestea deposit by Mumin *et al.* (1994). Generally, samples from the margin show higher Ag contents than those from the inner parts. The low Ag composition in the inner vein inhibits the observation of any well defined correlation with Cu; however, they show a negative correlation in samples from the margin, indicating a direct substitution between the two elements (Fig. 7A). The tetrahedrites are generally enriched in Zn over Fe with the Zn ranging from 0.78 to 1.66 atoms per formula unit (p.f.u), and Fe showing a wider range from 0.43 to 1.71 atoms p.f.u. The two elements show two distinct negative correlation patterns suggesting different conditions of crystallization or changing composition of the fluid (Fig. 7B). Zn and Fe substitution in type I is consistent with ideal stoichiometric composition with total Zn and Fe averaging 2.03 atoms p.f.u. All the analysed tetrahedrites showing ideal characteristics are Cu enriched with nearly 10 atoms p.f.u. Zn and Fe in the type II deviates from ideal stoichiometric composition with total Fe and Zn in excess of 2 atoms p.f.u. The general formula is represented approximately as $(Cu,Ag)_{9.61}(Fe,Zn)_{2.39}(Sb,As)_4S_{13}$.

Experimental work by Sack and Loucks (1985) demonstrated that (Fe-Cu) and (Zn-Cu) substitutions in tetrahedrites account for the Cu-deficiency in those tetrahedrites. A plot of Excess (Fe+Zn) against Cu (Fig. 8A) for Prestea tetrahedrites shows a well defined negative correlation consistent with the observation of Sack and Loucks. Fig. 8B however, illustrates that Fe substitution for Cu accounts for the Cu deficiency in the type II tetrahedrites at the Prestea deposit. Reaction of an Fe-bearing mineral assemblage with tetrahedrite to produce Cu-bearing species such as bournonite and chalcopyrite which are commonly associated with the tetrahedrites is most probable evidence for the Cu deficiency. In particular, at the vein margin where most of the tetrahedrites show non-ideal stoichiometry, chalcopyrite is the most dorminant Cu-bearing species and is most likely the controlling factor of Cu in the type II tetrahedrites. Tetrahedrites co-precipitated with gold exhibit ideal characteristics. This may suggest precipitation occurred during an equilibruim state of the mineralizing fluid. Further observation also indicates that the Ag composition in the tetrahedrites at Prestea is a function of the Fe/(Zn+Fe) ratio in the hydrothermal fluid, with Ag composition increasing with increasing Fe/(Zn+Fe), Fig. 9B.

Figure 9A shows a positive statistical correlation between Ag/(Ag+Sb) and Sb/(Sb+As). Sb shows a restricted range in the periphery compared with a relatively wider Sb range for the inner part of the vein. One tetrahedrite sample SQ28 from the inner vein at a depth of about 1200 m showed a relatively higher Ag and Sb content compared to the shallow samples. This shows that the Ag and Sb relationship varies in the same manner in the Prestea system. Thus, Ag compositions increase with increasing Sb

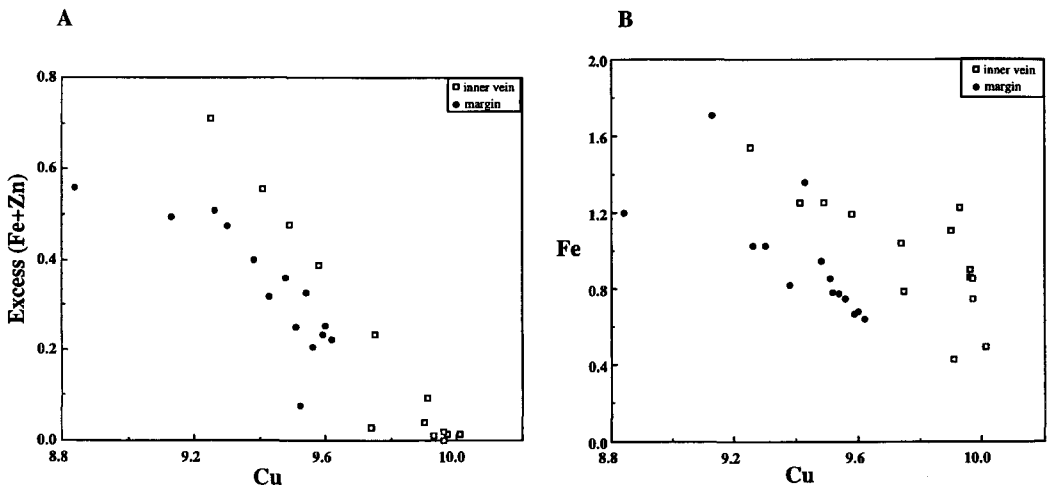

FIG. 8. Plots illustrating variation of (A) excess (Fe + Zn) and Cu, and (B) Fe and Cu in Prestea tetrahedrite.

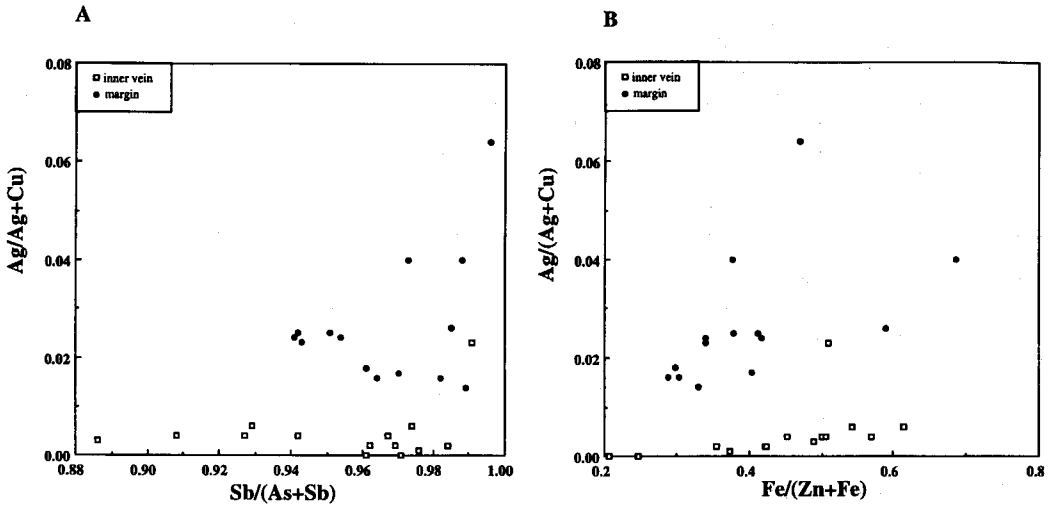

FIG. 9. Relationship between (A) Ag/(Ag + Cu) and Sb/(Sb + As), and (B) Ag/(Ag + Cu) and Fe/(Zn + Fe).

content. This observation may be consistent with the proposal by Mumin *et al.* (1994) which indicated reducing Ag and Sb contents in tetrahedrite with fluid ascent. The higher Sb and Ag contents in peripheral zones at Prestea are also consistent with general observations (e.g. Wu and Petersen,1977; Hackbarth and Petersen, 1984), an indication of early crystallization of the marginal tetrahedrites. The total As and Sb in all analysed grains is nearly constant with average of 4.02 atoms per formula unit. The relationship between the two elements indicates a coupled substitution.

Genesis of the ore minerals

Based on the ore textures observed under reflected light and electron microprobe analyses, three possible paragenetic stages can be recognized (Fig. 10).

Faulting and fissuring initiated stage I of the mineralization accompanied by the formation of chalcopyrite, pyrrhotite, pyrite (type III) and arsenopyrite. The early precipitation of the sulphide-rich phases and local disequilibruim between the As-bearing fluid and crystallizing arsenopyrite resulted in the progressive increase in As content from core to rim of the arsenopyrite.

Stage II is composed of two phases, IIa and IIb, and forms a prolonged and main stage of the ore mineralization. This stage affected most minerals of stage I through mobilization and recrystallization, as well as the precipitation of new minerals including native gold. Stage IIa was marked by a period of fracturing and the subsequent introduction of new pulse of hydrothermal fluid with elevated activities of As and Au complexes, subordinate concentration of Pb, Sb, Ni and Co leading to the precipitation of Co-rich pyrite (type I), arsenopyrite, As-rich pyrite (type II), and sphalerite in that sequence. Stage IIb represents the later phase of stage II, characterized by an increase in the Sb and Pb concentrations. Tetrahedrites were the first Sb-bearing ores to be precipitated in the sequence followed by the precipitation of the Pb-Sb sulphosalts boulangerite, bournonite and jamesonite, and finally galena.

Stage III formed the final stage of mineralization with the ore fluid depleted of trace elements and further precipitation of type III pyrite and some chalcopyrite and sphalerite.

Discussion

The ore mineral assemblage at Prestea reflects the relatively reducing condition of the fluid. A decreasing trend of As content from the core to the rim of the As-rich type II pyrite, and the lack of As in type III pyrite, which in some cases occurs as overgrowths on the type II pyrites, gives an indication of an increase in As concentration in the fluid from stage I as the mineralization progressed. The paragenetic sequence further suggests the As activity attained maximum value during stage IIa of the mineralization.

The occurrence of As-rich pyrites has been reported by many authors in gold deposits (Arehart *et al.*, 1993; Dill *et al.*, 1995; Fleet *et al.*, 1989; Rytuba, 1985) and in high temperature geothermal systems (Ballantyne

TABLE 2. Microprobe analyses of tetrahedrites. (No. of atoms based on Cu+Ag+Fe+Zn=12)

Inner vein														
Sample	SQ2-1	SQ2-2	SQ2-3	SQ2-4	SQ2-2	SQ3-5	SQ3-6	SQ7-1	SQ7-2	SQ7-3	SQ7-4	SQ7-5	SQ7-6	SQ 28
No. of analysis	3	2	2	1	1	2	3	3	3	2	3	3	2	2
Element (wt %)														
Cu	37.40	36.42	37.40	37.12	36.10	37.03	37.81	37.82	37.86	37.83	38.07	37.94	38.05	36.27
Ag	0.02	0.22	0.22	0.23	0.26	0.14	0.38	0.12	0.09	0.40	0.02	0.23	0.10	1.44
Fe	1.45	4.26	4.10	4.31	5.30	2.65	4.13	2.86	2.51	3.72	1.64	3.02	2.85	3.39
Zn	6.44	5.20	4.80	4.93	4.67	5.62	3.04	4.55	4.93	3.66	5.85	4.30	4.57	3.80
As	0.54	2.10	1.33	1.03	1.63	0.29	1.30	0.56	0.44	0.47	0.72	0.60	0.71	0.17
Sb	29.35	26.50	27.32	27.10	26.01	29.24	27.90	28.94	29.11	28.94	28.94	28.90	28.67	29.10
S	25.36	25.87	25.46	25.69	25.87	24.74	24.79	24.91	24.92	24.92	25.12	24.98	24.99	24.38
Total	100.56	100.56	100.62	100.39	100.03	99.83	99.35	99.82	99.90	99.97	100.42	99.98	99.95	98.60
Number of atoms														
Cu	9.91	9.41	9.58	9.49	9.25	9.75	9.93	9.96	9.97	9.90	10.01	9.96	9.97	9.74
Ag	0.00	0.03	0.03	0.03	0.04	0.02	0.06	0.02	0.01	0.06	0.00	0.04	0.02	0.23
Fe	0.43	1.25	1.19	1.25	1.54	0.79	1.23	0.86	0.75	1.11	0.49	0.90	0.85	1.04
Zn	1.66	1.31	1.19	1.22	1.16	1.44	0.78	1.16	1.26	0.93	1.50	1.10	1.17	0.99
As	0.12	0.46	0.29	0.22	0.35	0.07	0.29	0.13	0.10	0.10	0.16	0.13	0.16	0.04
Sb	4.06	3.57	3.65	3.62	3.48	4.02	3.83	3.98	4.00	3.95	3.97	3.96	3.92	4.08
S	13.31	13.25	12.92	13.02	13.14	12.91	12.91	13.00	13.01	12.93	13.09	13.01	12.98	12.98
Cu+Ag	9.91	9.44	9.61	9.52	9.29	9.77	9.99	9.98	9.98	9.96	10.01	10.00	9.98	9.97
Fe+Zn	2.09	2.56	2.39	2.48	2.71	2.23	2.01	2.02	2.02	2.04	1.99	2.00	2.02	2.03
As+Sb	4.18	4.03	3.94	3.84	3.83	4.08	4.12	4.10	4.10	4.06	4.13	4.10	4.08	4.12

TABLE 2. *Contd*

Vein boundary with host rock

Sample	BV1-2	BV1-3	BV1-4	BV1-5	BV1-6	BV2-1	BV2-2	BV2-3	BV2-5	BV4(1-3)	BV4-4	BV4-5	BV4-11	BV4-8
No. of analysis	1	2	2	1	3	2	1	1	1	3	1	1	1	1
Element (wt.%)														
Cu	33.14	35.40	34.88	36.72	36.38	35.93	36.63	36.01	36.16	36.23	36.13	36.58	36.20	36.36
Ag	3.83	1.54	2.45	0.97	1.00	2.55	1.16	1.56	1.66	1.43	1.52	0.86	1.51	1.06
Fe	3.95	3.47	5.75	2.30	2.13	2.60	2.24	2.84	4.60	2.77	3.53	2.59	2.50	3.21
Zn	5.24	5.80	3.07	6.18	6.15	5.02	6.15	5.44	3.76	6.29	5.77	6.14	5.67	5.55
As	0.07	1.04	0.21	0.65	0.32	0.48	0.72	0.88	0.28	1.02	1.05	0.19	0.83	0.54
Sb	28.07	27.17	28.57	28.28	28.63	28.72	28.77	27.95	29.15	27.30	27.03	28.77	27.66	28.67
S	25.29	26.02	25.56	25.67	25.47	24.79	24.95	25.11	25.02	25.13	25.44	25.45	25.21	25.16
Total	99.59	100.44	100.48	100.76	100.09	100.09	100.62	99.79	100.63	100.17	100.46	100.57	99.57	100.55
Number of atoms														
Cu	8.84	9.26	9.13	9.60	9.62	9.52	9.59	9.51	9.43	9.38	9.30	9.54	9.56	9.48
Ag	0.60	0.24	0.38	0.15	0.16	0.40	0.18	0.24	0.26	0.22	0.23	0.13	0.23	0.16
Fe	1.20	1.03	1.71	0.68	0.64	0.78	0.67	0.85	1.36	0.82	1.03	0.77	0.75	0.95
Zn	1.36	1.47	0.78	1.57	1.58	1.29	1.57	1.40	0.95	1.58	1.44	1.56	1.46	1.41
As	0.01	0.23	0.05	0.14	0.07	0.11	0.16	0.20	0.06	0.22	0.23	0.04	0.19	0.12
Sb	3.91	3.72	3.90	3.86	3.95	3.97	3.93	3.85	3.97	3.69	3.63	3.92	3.81	3.90
S	13.37	13.45	13.26	13.30	13.35	13.02	12.95	13.14	12.93	12.90	12.97	13.16	13.20	13.00
Cu+Ag	9.44	9.49	9.51	9.75	9.78	9.92	9.77	9.75	9.68	9.60	9.52	9.68	9.79	9.64
Fe+Zn	2.56	2.51	2.49	2.25	2.22	2.08	2.23	2.25	2.32	2.40	2.48	2.32	2.21	2.36
As+Sb	3.92	3.95	3.95	4.00	4.02	4.08	4.09	4.05	4.03	3.91	3.86	3.96	4.00	4.02

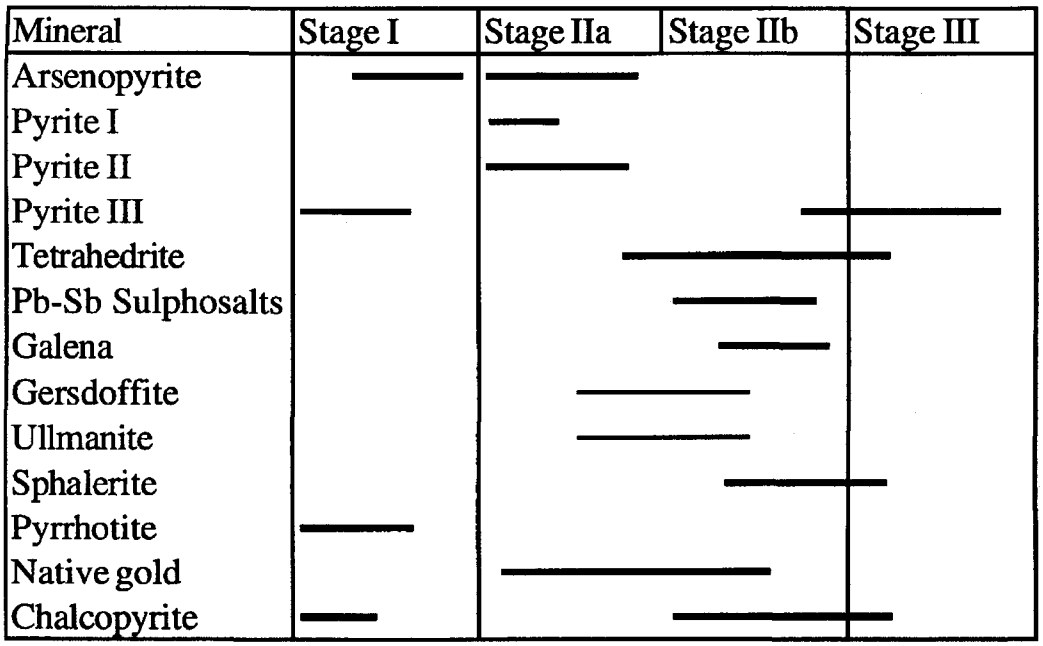

FIG. 10. Paragenesis of ore minerals at the Prestea gold deposit.

and Moore, 1988). The mechanism of formation of the As-rich pyrites is scarcely documented. Fleet *et al.* (1989) concluded that As is incorporated as a metastable solid solution in pyrite. Ballantyne and Moore (1988) attributed it to a redox disequilibruim reaction between the As-bearing ore fluid and crystallizing pyrites. Rytuba (1985) and Dill *et al.* (1995) stated that As-rich pyrite at the Carlin-type and Kharma gold deposits, were the result of As coating on pyrite surfaces. At Prestea, the textural relationship of the As-rich pyrites suggest a combination of the above mechanisms is likely to account for the dominant occurrence of As-rich pyrite.

Oscillatory zoning is a common feature in the arsenopyrite and As-rich pyrite at Prestea, indicating an episodic flow of hydrothermal fluid during mineralization or a disequilibrium between growing mineral and adjacent fluid during crystallization (e.g. Fleet *et al.*, 1989; Sibson *et al.*, 1988). Such a mechanism for oscillatory zoning is evident by the occurrence of oscillatory composition of As in arsenopyrite and As-rich pyrite. Yardley *et al.* (1991), however, gave another plausible mechanism attributed to changes in the activity of the involved species in the fluid, as a consequence of rapid changes in the fluid oxidation state.

This mechanism may explain the oscillatory pattern of Ni observed in some As-rich pyrite and arsenopyrite at Prestea, where microscale zones of Ni alternate within both minerals (Fig. 5). The positive correlation of Ni and As, as illustrated in Fig. 6A also indicates a symphathetic relationship between the two elements in the ore fluid. A local fluctuation of As and Ni activity ratio due to rapid changes in the redox state of the ore fluid is attributed to such an oscillatory zoning. This could be triggered by episodic pressure release during fracturing and fissuring.

Acknowledgements

We express our sincere appreciation to H. Shimazaki for an initial review of the manuscript, and to S. Maruyama and Y. Isozaki for their encouragement and support during this research. We are also indebted to M. Shimizu and A. Imai for their suggestions and assistance. A review by R.J. Herrington greatly improved this manuscript. NQH was support financially by the Japanese Ministry of Education (Monbusho).

References

Arehart, G.B., Chyrssoulis, S.L. and Kesler, S.E. (1993) Gold and arsenic in iron sulphides from sediment-hosted disseminated gold deposits: Implications for

depositional processes. *Econ. Geol.*, **88**, 171–85.

Ballantyne, J.M. and Moore, J.N. (1988) Arsenic geochemistry in geothermal systems. *Geochim. Cosmochim. Acta*, **52**, 475–83.

Black, R. (1980) Precambrian of West Africa. *Episodes*, **4**, 3–8

Bowell, R.J. (1992) Supergene gold mineralogy at the Ashanti, Ghana: Implications for the supergene behaviour of gold. *Mineral. Mag.*, **56**, 545–60.

Davies, D.W., Hirds, W., Schaltegger, U. and Nunoo, E.A. (1994) U-Pb age constraints on deposition and the provenance of Birimian and gold-bearing Tarkwain sediments in Ghana, West Africa. *Precamb. Res.*, **67**, 89–107.

Dill, H.G., Weiser, T., Bernhardt, I.R. and Kilibarda, R.C. (1995) The composite gold-antimony vein gold deposit at Kharma (Bolivia). *Econ. Geol.*, **90**, 51–66.

Eisenlohr, B.N. (1992) Conflicting evidence on the timing of mesothermal and palaeoplacer gold mineralization in early Proterozoic rocks from southwestern Ghana, West Africa. *Mineral. Deposita.*, **27**, 23–9.

Eisenlohr, B.N. and Hirdes, W. (1992) The structural development of the early Proterozoic Birimian and Tarkwaian rocks of southwestern Ghana, West Africa. *J. African Earth Sci.*, **14**, 313–25.

Fleet, M.E., MacLean, P.J. and Barbier, J. (1989) Oscillatory-zoned As-bearing pyrites from strata-bound gold deposits: An indication of the fluid evolution. *Econ. Geol. Mon.*, **6**, 356–362.

Hackbarth, C.J. and Petersen, U. (1984) A fractional crystallization model for the deposition of argentian tetrahedrite. *Econ. Geol.*, **79**, 448–60.

Hammond, N.Q., and Shimazaki, H. (1994) Geology and geochemical aspects of ore formation at the Prestea mesothermal vein gold deposit in the Birimian system of Ghana. *Internat. Geol. Review*, **36**, 715–31.

Hawley, J.E. and Nichol, I. (1961) Selenium in some Canadians sulfides. *Econ. Geol.*, **54**, 467–87.

Hirdes, W., Davis, D.W. and Eisenlohr, B.N. (1992) Reassessment of Proterozoic granitoid ages in Ghana on the basis of U/Pb zircon and monazite dating. *Precamb. Res.*, **56**, 89–96.

Hutchison, M.N. and Scott, D.S. (1981) Sphalerite geobarometry in the Cu-Fe-Zn-S system. *Econ. Geol.*, **76**, 143–53.

Johnson, N.E., Craig, J.R. and Rimstidt, J.D. (1986) Compositional trends in tetrahedrite. *Canad. Mineral.*, **24**, 385–97.

Kesse, G.O. (1985) *The Mineral and Rock Resources of Ghana*. Balkema, Rotterdam, 610pp.

Leube, A., Hirdes, W., Mauer, R. and Kesse, G.O. (1990) The early Proterozoic Birimian Supergroup of Ghana and some aspects of its associated gold mineralization. *Precamb. Res.*, **46**, 139–65.

Lynch, J.V.G (1989) Large-scale hydrothermal zoning reflected in the tetrahedrite-freibergite solid solution, Keno Hill Ag-Pb-Zn district, Yukon. *Canad. Mineral.*, **27**, 383–400.

Miller, W.J. and Craig, J.R (1983) Tetrahedrite-tennantite series compositional variations in the Cofer deposit, Mineral district, Virginia. *Amer. Mineral.*, **68**, 227–34.

Mucke, A. and Dzigbodi-Adjimah (1994) Ore textures and parageneses of the Prestea and Obuasi gold deposit in the Ashanti Belt of Ghana: An ore microscopy study. In *Metallogenesis of Selected Gold Deposits in Africa* (T. Oberthur, ed.). *Geologisches Jahrbuch Reihe*, **100**, 167–99.

Mumin, A.H., Fleet, M.E. and Chryssoulis, S.L. (1994) Gold mineralization in As-rich mesothermal gold ores of the Bogosu-Prestea mining district of the Ashanti gold belt, Ghana: remobilization of 'invisible' gold. *Mineral. Deposita*, **29**, 445–60.

Ntiamoah-Agyakwa, Y. (1979) Relationship between gold and manganese mineralization in the Birimian of Ghana, West Africa. *Geol. Mag.*, **116**, 345–52.

O'Leary, M.J. and Sack, R.O. (1987) Fe–Zn exchange reaction between tetrahedrite and sphalerite in natural environments. *Contrib. Mineral. Petrol.*, **96**, 415–25.

Oberthur, T., Vetter, U., Mumm, A.S., Weiser, T., Amanor, J.A., Gyapong, W., Kumi, R. and Blenkinsop, T.G. (1994) The Ashanti gold deposit at Obuasi: Mineralogical, geochemical, stable isotope and fluid inclusion studies on the metallogenesis of the deposit. In *Metallogenesis of Selected Gold Deposits in Africa* (T. Oberthur, ed.). *Geologisches Jahrbuch Reihe*, **100**, 31–131.

Rytuba, J. (1985) Geochemistry of hydrothermal transport and deposition of gold and sulfide minerals in Carlin-type gold deposit. *U.S. Geol. Surv. Bull.*, **1646**, 27–34.

Sack, R.O. and Loucks, R.R. (1985) Thermodynamic properties of tetrahedrite-tennantites: constraints on the interdependence of Ag–Cu, Fe–Zn, Cu–Fe, and As–Sb exchange reactions. *Amer. Mineral.*, **70**, 1270–89.

Sibson, R.H., Robert, F. and Poulsen, K.H. (1988) High-angle reverse faults, fluid-pressure cycling, and mesothermal gold-quartz deposits. *Geology*, **16**, 551–5.

Slim-shimi, N., Moëlo, Y., Tlig, S. and Lévy, C. (1996) Sulfide geochemistry and genesis of Chouichia and Ainel Bey copper deposits in northwestern Tunisia. *Mineral. Deposita*, **31**, 188–200.

Taylor, P.N., Moorbath, S., Leube, A. and Hirdes, W. (1992) Early Proterozoic crustal evolution in the Birimian of Ghana, Constraints from geochronology and isotope geochemistry. *Precamb. Res.*, **56**, 97–111.

Wu, I. and Petersen, U. (1977) Geochemistry of

tetrahedrite and mineral zoning at Casapalca, Peru. *Econ. Geol.*, **72**, 993–1016.

Yardley, B.W.D., Rochelle, C.A., Barnicoat, A.C. and Lloyd, G.E. (1991) Oscillatory zoning in metamorphic minerals: an indicator of infiltration metasomatism. *Mineral. Mag.*, **55**, 357–65.

[*Manuscript received 30 September 1996: revised 12 June 1997*]